Publised in CHEMCATCHEM Volume 7, Issue 8, pages 1347–1356, April 20, 2015

Function of support and metal loading on catalytic CO_2 reduction using Ru nanoparticles supported on carbon nanofibers

Laura Roldán, Yanila Marco, Enrique García-Bordejé*

Instituto de Carboquímica (ICB-CSIC), Miguel Luesma Castán 4, E-50018 Zaragoza, Spain,

Abstract

Catalytic CO_2 reduction has been performed using carbon nanofibers or nitrogen doped carbon nanofibers as novel support for several Ru contents. The catalyst consisting of 5 wt% Ru on nitrogen doped carbon nanofiber exhibited the highest conversion at relatively low temperature, complete selectivity to CH_4 and stable catalytic performance. The catalytic performance was substantially superior to catalysts supported on carbon nanotubes and akin to the best metal oxide supported catalyst in the literature. The characterisation of the prepared catalyst by transient experiments (CO_2-TPD, TPSR and transient response to CO_2 removal) revealed that the catalyst support participates actively in the reaction. The Ru content governed the selectivity, either favouring CO formation for lower Ru contents (0.5-2 wt%) or CH_4 formation for 5 wt% Ru loading. The mean Ru particle size determined by TEM was similar for the several metal loadings. Therefore, the substantially different selectivity patterns cannot

* Corresponding author: Tel.:+ 34 976733977; fax.: +34 976733318 *E-mail address:* jegarcia@icb.csic.es

be attributed to structure sensitivity. The higher selectivity to CH_4 can be explained by the enhanced supply of 4 H_{ad} to the activated CO_{ad} intermediate, which was demonstrated to be the rate determining step.

Keywords: carbon nanofibers, nitrogen doping, catalyst support, ruthenium nanoparticles, CO_2 hydrogenation, reaction mechanism.

1. Introduction

The perceived risk of running out of conventional fossil fuels and the pollution risks associated with burning fuels led the boom in programs for developing renewable energy. The efficient utilization of renewable energy sources from wind turbines and solar panels is still an ongoing challenge. Naturally, power generated by renewable energies (wind, photovoltaics) are intermittent, highly volatile and not in line with the demand of electricity. Electricity from wind and sun is generated at irregular intervals and the energy is produced at locations where it is not directly consumed. Only the large-scale storage of energy can reliably secure an economic supply from renewable sources. Thus, solutions for long-range transportation and storage of renewable energies are currently of great interest.[1]

Recently, much interest has been devoted to energy conversion based on the hydrogen cycle ("hydrogen economy") such as water splitting. It is easy and affordable to convert electricity to hydrogen via electrolysis, a proven technology in the chemical industry.[2] The main unsolved problem of H_2 as energy carrier is its storage. Hydrogen can be stored and used in the existing gas infrastructure but the discharge time is typically lower than 100 hours, depending on technical regulations. Research is being undertaken to widen the use of hydrogen in the existing gas infrastructure. When it is a need of long temporary storage it is possible to convert H_2 with CO_2 into Synthetic Natural Gas

(CH_4).[3] Synthetic Natural Gas can be stored and used in the existing gas infrastructure without limitation. This fact has the additional advantage that the gas infrastructure (transport, storage and distribution) is immediately available and there is no investment needed. This will allow also the transportation of energy from areas with high renewable power (sun or wind rich) to remote areas with less renewable energy. A cost estimation study of a CO_2 recycling system producing CH_4 using photovoltaic energy in Middle East and transporting it to Japan found that the cost of energy input of CO_2 recycling is similar to the obtaining of LNG from wells (mining, liquefaction and purification).[4] Moreover, 79 % of CO_2 emissions form a 1 GW CH_4-combustion power plant can be reduced by CO_2 conversion to CH_4 when CO_2 is recovered at the power plant. The conversion of CO_2 into fuels and useful chemicals using renewable H_2 will permit that the carbon-cycle, which has generally an open end due to burning of fossil fuels and release as CO_2 into atmosphere, can be closed by capturing CO_2 in the power station and recycling it to fuel. Thus, this approach allows killing two birds with a stone, the storage of renewable H_2 and the reduction of CO_2 emissions. Several projects are currently run worldwide exploiting this concept of green natural gas such as the "e-gas" by Audi or "Power2gas" by E.ON.

The reaction of CO_2 and H_2 was first reported a century ago and it is known as the Sabatier reaction.[5] It has been more intensively investigated recently, due to fundamental and practical significance in the context of catalysis, surface science, biology, nanotechnology and environmental science.[6,7] Photocatalysis, electrocatalyst[7] and thermal homogeneous[6, 8] and heterogeneous catalysts have been used to hydrogenate CO_2. State of the art photocatalysts used in artificial photosynthesis produce low CO_2 conversions rendering the process inefficient thus far.[9] Homogeneous catalysts show satisfactory activity and selectivity, but the recovery and regeneration are problematic. Alternatively, heterogeneous catalysts are preferable in terms of stability, separation, handling, reuse and reactor design, reducing the costs for large-scale productions. Regarding heterogeneous catalysis, supported transition metals Ni [10-13]and Co[14, 15] and noble metals including Ru,[16-18] Pd,[19] Pt,[19, 20] and Rh,[19, 21-23] are active for this reaction. The support plays an important role in the catalytic reaction as it may interact with the reactant(s), stabilize intermediates or reaction products or create special interfacial sites where reactions can proceed. Support can have electronic effects on the catalytic nanoparticle[24] or it can adsorb some of the reactants increasing the local concentration of the reactant.[25] Accordingly, some reactions have been reported to take place in the interphase between metal and support.[26, 27] Several support materials have been used in CO_2 hydrogenation such as alumina,[28-31] titania,[27, 32, 33] titanium carbide,[34] silica,[15] ceria, [12, 18, 35] zeolite,[24] or carbon materials such as activated carbon[36] or carbon nanotubes.[37, 38]

CO_2 reduction is reported to require a bifunctional catalyst, *i.e.* one function to activate CO_2 and another to activate H_2. Park and MacFarland[19] observed a selectivity shift from CO to CH_4 by modifying Pd on SiO_2 with MgO, while MgO/SiO_2 showed no measurable activity. They rationalized their results suggesting a bifunctional mechanism in which CO_2 first strongly adsorbs onto MgO inhibiting CO desorption, while Pd dissociates H_2. There are also clear evidences that CO_2 interacts with Al_2O_3 support to produce alumina-bound carbonates/bicarbonates.[31, 39] Therefore, metal oxide supports are clearly not innocent in this reaction. On the other hand, CNT is usually considered as an inert support material. In fact, when using CNT as Ru support for CO_2 hydrogenation, the activity was negligible, which was attributed to the lack of the function to activate CO_2.[40] To the best of our knowledge, Ru on carbon nanofibers (CNF) has not been studied for CO_2 methanation.

Herein, we used CNF and nitrogen doped CNF (N-CNF) as support for several Ru loadings. The catalyst showed remarkable activity in CO_2 hydrogenation, in contrast to previous reports using CNT as support. This prompted us to study the mechanism of reaction. Since in-situ spectroscopic characterisation is not usually performed using carbon-based catalysts because it is hampered by high absorbance of carbon, the mechanism of reaction was studied here by catalytic transient response. This characterisation enabled to explain the effect of support and metal loading on the excellent selectivity to CH_4. It was revealed that the support played an active role in the reaction, which lends the catalyst an outstanding performance compared to metal oxide supported ones.

2. Experimental

2.1. Catalyst preparation

CNFs were grown on a 20 wt% Ni on alumina catalyst prepared by incipient wetness impregnation of nickel nitrate on alumina (Pural, Sasol) and calcined at 873 K in N_2 flow. The powder catalyst was placed on a porous frit of a vertical reactor. After reducing the catalyst at 823 K using 100 ml/min of H_2:N_2 mixture during 1 h, the CNFs growth was carried out at 873 K using 100 ml/min of a C_2H_6:H_2 mixture (50:50). N-CNF were grown on a 20 wt% Fe on alumina catalyst prepared by incipient wetness impregnation of iron nitrate on alumina (Pural, Sasol) and calcined at 873 K in N_2 flow. The catalyst was reduced at 823 K using 100 ml/min of a H_2:N_2 (50:50) mixture during 1 hour. Subsequently, the reactor was heated to the growth temperature (1023 K) under Ar. After reaching the temperature, the reaction mixture was admitted. The reaction mixture consisted of 100 ml/min Ar mixed with 0.15 ml/min of ethylendiamine (10 ml in total) fed using a syringe. The ethylenediamine in argon mixture passed through an evaporator at 473 K and a heated line to the reactor containing the growth catalyst.

Both CNFs and N-CNFs supports were purified from the growth catalyst under reflux of NaOH (5M) for 4 h at 353 K and later under reflux of HCl at 373 K for another 4 h. After HCl treatment, thorough rinsing with distilled water was carried out until neutrality of the filtrate. After this purification process, the residual catalyst was less than 1 wt% as determined by oxidation in thermobalance and no HCl traces were detected by XPS.

The preparation of ruthenium catalysts was performed by incipient wetness impregnation. The CNF or N-CNF supports were crushed to powders of particle size smaller than 200 µm. The desired amount of Ru nytrosil nitrate ($Ru(NO)(NO_3)$) was dissolved in an ethanol:water mixture (4:1) and impregnated in the catalysts to achieve different Ru loadings (0.5, 2, 5 wt%) with respect to the total sample. After drying, the catalyst was first calcined in N_2 at 723 K using a heating rate of 1 K/min and subsequently reduced in H_2 at the same temperature and heating rate. The reduced catalysts have been denoted as *loading*%Ru/*support*. The actual Ru content on the catalyst was analysed by ICP-OES.

2.2. Catalytic tests and characterisation

Catalytic testing was carried out in a continuous-flow 6 mm i.d. quartz reactor inside vertical furnace with a temperature controller (Eurotherm). 50 mg of catalyst diluted in SiC were placed on quartz wool inside the reactor. Prior to catalytic test, the catalyst was heated to 723 K in N_2 flow using a heating ramp of 10 K/min and it was reduced with 100 ml/min of H_2:N_2 (50:50) at 723 K for 0.5 h. The reaction temperature was controlled with a thermocouple inside the catalytic bed. The reaction conversion and selectivities were recorded at steady state using 60 ml/min of a reaction mixture consisting of 5 % CO_2, 15 % H_2 and Ar to balance. This flow rate gives rise to a space velocity of 19000 h^{-1}. Gas analysis was performed with a Pfeiffer vacuum mass spectrometer. The following m/z signals were recorded in mass spectrometer: 2, 16, 18, 28, 40, 44. The signals of the gases were calibrated taking into account the baseline of Ar and the fragmentation pattern of each mass. The main m/z signals used for each gas were m/z= 2 (H_2), m/z= 16 (CH_4), m/z= 18 (H_2O), m/z= 28 (CO), m/z= 40 (Ar), m/z= 44 (CO_2). The concentration of CO was calculated subtracting the contribution of CO_2 to m/z=28. The concentration of CH_4 was calculated subtracting the contribution of CO_2 and CO to m/z=16. The correct calibration of the mass spectrometer was double-checked analysing the gases by calibrated Agilent Micro GC 3000A. Stability tests were conducted in the same conditions but leaving the reaction overnight.

The transient response behaviour of reactant and products to the sudden removal of CO_2 from reactant gas under isothermal reaction conditions was studied. To this end, after recording reaction at steady state using a feed gas consisting of 5% CO_2, 15% H_2, Ar to balance, CO_2 was suddenly removed from the reaction mixture and the total flow rate was kept constant by completing the balance with Ar. The dead volume at the outlet line to the mass spectrometer was determined to be negligible. Therefore, all the changes in the mass spectrometer signals reflected accurately the changes of the gases in contact with the catalyst.

Temperature-programmed desorption (TPD) and temperature-programmed surface reaction (TPSR) experiments were conducted as follows. The catalyst was heated to 723 K at a heating rate of 10 K/min in inert gas. At this temperature, it was reduced with 100 ml/min of H_2:N_2 mixture for 0.5 h. The reactor was allowed to cool down until 298 K and CO_2 was flushed for 0.5 h. The gas was switched to 100 ml/min Ar and it was kept during 1 h to remove weakly physisorbed CO_2. Then the gas was adjusted to 60 ml/min of Ar for TPD experiments or to 60 ml/min 15% H_2 in Ar for TPSR experiments. When the signal in mass spectrometer was stabilised, the temperature was raised until 723 K at a rate of 10 K per minute while monitoring the desorbed gases.

Ru metal nanoparticle size on carbon nanofibers was measured by scanning transmission electron microscopy (STEM) using a FEI TECNAI F30 electron microscope equipped with Gatan Energy Filter and cold field emission gun (FEG) operated at 300 kV with 1.5 Å lattice resolution. TEM specimens were prepared by ultrasonic dispersion in ethanol of powder catalyst. A drop of the suspension was applied to a holey carbon support grid. The particle size distribution was calculated by statistical analysis of 400 particles in ~20 images on CNFs. Mean Ru particle size evaluated as the Surface area weighted diameter ($\overline{d}_{Ru}$) was computed according to the following equation:

$$\overline{d}_{Ru} = \frac{\sum_i n_i d_i^3}{n_i d_i^2}$$

Where n_i represents the number of particles with diameter $d_i (\sum_i n_i \geq 400)$

3. Results

3.1. Catalytic testing

Figures 1 A-C show the CO_2 conversion, CH_4 and CO yields, respectively, for three different Ru loadings on CNF and N-CNFs. There are very significant differences in terms of conversion and selectivity as a function of the loading, irrespective of the support either CNFs or N-CNFs. Comparing the performance of 0.5 wt% and 2 wt% Ru loaded catalysts, the differences in CO_2 conversions are very modest or even inexistent for CNF and N-CNF supported catalyst, respectively. The CO_2 conversion increases significantly as loading does from 2 to 5 wt% Ru. The catalysts containing 5 wt% Ru achieve thermodynamic equilibrium at around 620 K. Comparing the two supports, the 5%Ru/N-CNF provided larger conversion than 5%Ru/CNF. The rise of conversion as metal loading increases can be easily rationalized on the basis of a larger number of sites to activate CO_2. However, the effect of loading on selectivity is still more noticeable and not that straightforward to explain. The selectivity to CH_4 increases substantially as the metal loading increases (Figure 1B). The highest selectivity to CH_4 corresponds to 5%Ru/N-CNF, which exhibited selectivity to CH_4 between 90-97 % in all the range of studied temperatures (up to 670 K). The onset of CO occurs at around the same temperature (~520 K) for all catalysts (Figure 1C). The CO yield increases as the temperature rises and it is observed a peak maximum at temperatures around that of the onset of CH_4 evolution (Figure 1B). For temperatures above the onset of CH_4, the CO yield decreases or remains stable. For this reason, the catalyst for which the onset in CH_4 evolution occurs at the lowest temperature, *i.e.* 5%Ru/N-CNF, the CO yield remains at negligible values in all the range of temperatures. For the highest tested temperatures, some catalysts exhibited a slight increase of CO and a decrease of CH_4, which may be attributed to the thermodynamic equilibrium. Since the hydrogenation of CO_2 is highly exothermic ($\triangle H$=-164 KJ/mol), at higher temperatures, the thermodynamic equilibrium favours steam reforming of CH_4 and reverse water gas shift, which are endothermic processes and lead to the production of CO.[29] Thus, these reactions are responsible for the small rise of the CO yield at the highest temperatures. We decided to keep reaction temperatures below 673 K to avoid these undesired reactions and also the gasification of the support that was found for temperatures > 650 K as revealed in TPSR experiment shown below.

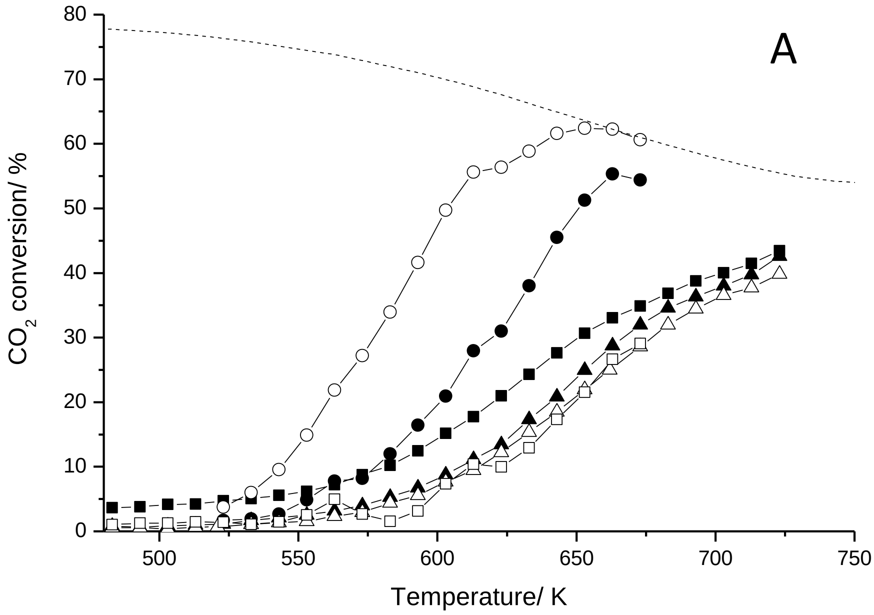
A
80
70
60
50
40
30
20
10
0
500
550
600
650
700
750
CO_2 conversion/ %
Temperature/ K

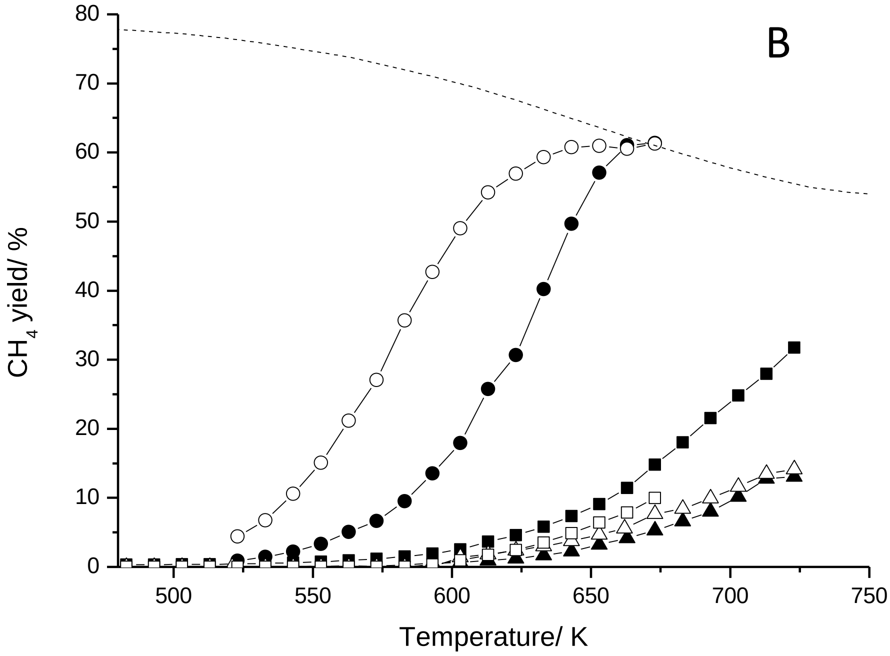
B
80
70
60
50
40
30
20
10
0
500
550
600
650
700
750
CH_4 yield/ %
Temperature/ K

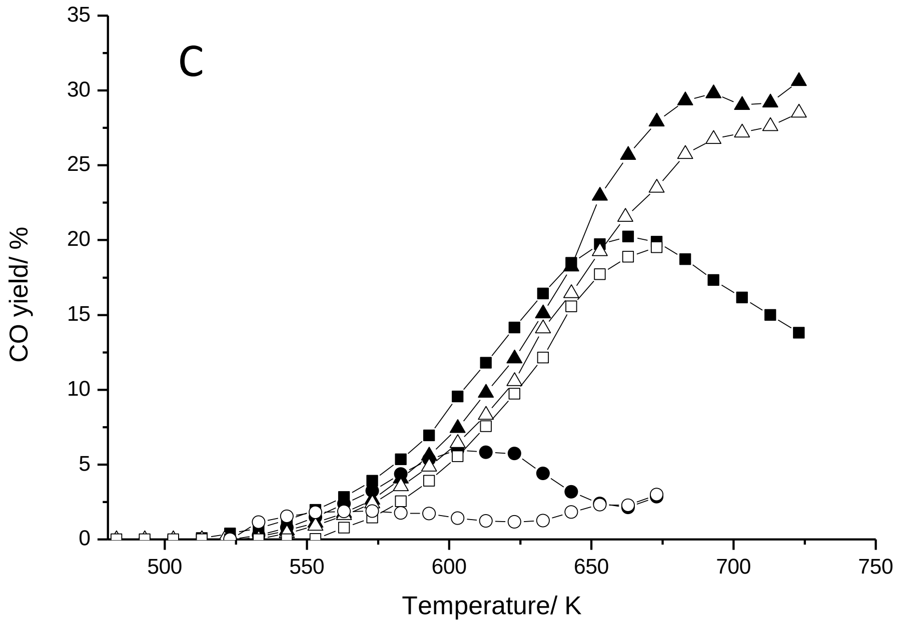

Figure 1. CO_2 conversion (A), CH_4 yield (B) and CO yield (C) for different Ru loaded catalyst on CNF and N-doped CNF: (▲) 0.5%Ru/CNF, **(■)** 2%Ru/CNF, (●) 5%Ru /CNF, **(△)** 0.5%Ru/N-CNF, **(□)** 2%Ru/N-CNF, **(○)** 5%Ru/N-CNF. The dotted line represents values at thermodynamic equilibrium.

Table 1 shows turnover rates, CH_4 productivity and space time yield at 673 K for all the tested catalysts. The catalysts containing 0.5% Ru exhibited the highest turnover but the CH_4 productivity per Ru mol is in the same range as for the other Ru loadings. The space time yield (STY) per catalyst weight increases proportionally as loading increases. Thus, the highest STY value at 673 K was achieved using 5%Ru/N-CNF as catalyst.

Table 1. Turnover rates at two temperatures and space time yield at 673 K

	Turnover rate	CH_4 productivity	Space time yield

	at 673 K mol_{Conv} $(mol_{Ru})^{-1}$ s^{-1}	at 673 K mol_{CH4} $(mol_{Ru})^{-1}$ s^{-1}	(STY) at 673 K Kg_{CH4} $(Kg\ cat)^{-1}$ h^{-1}
0.5% Ru/CNF	0.30	0.04	0.13
2%Ru/CNF	0.07	0.03	0.37
5%Ru/CNF	0.05	0.05	1.42
0.5% Ru/N-CNF	0.26	0.06	0.20
2%Ru/N-CNF	0.06	0.02	0.23
5%Ru/N-CNF	0.05	0.05	1.54

To get some insight into the reaction mechanism, transient experiments were performed. First, we performed temperature programmed desorption (TPD) in Ar flow after adsorption of CO_2 at room temperature on the catalyst prereduced at 723 K and flushed with Ar at room temperature to remove weakly physisorbed species. All the catalysts showed similar TPD profiles. Representative TPD profiles corresponding to 5%Ru/N-CNF are shown in Figure 2. The formation of H_2O peaked at 400 K indicates that there was hydrogen and oxygen adsorbed on the catalyst surface. H_2 should come from dissociative adsorption of H_2 on metal surface during reduction step that was not removed during flushing with Ar. Oxygen should come from the dissociative adsorption of CO_2 into O_{ad} and CO_{ad} on the catalyst surface. Some very small amount of CH_4 seems to be formed from reaction of chemisorbed H_{ad} and CO_{ad} species. The CO_2 profile shows desorption peaks at around 350 K and at 700 K, which may be attributed to physisorbed CO_2 and some CO_2-desorbing oxygenated groups, respectively, formed in CO_2 adsorption stage. There is no CO desorption in all the range of temperatures, indicating that CO_{ad} species formed by CO_2 dissociation are very strongly adsorbed on the catalyst/support.

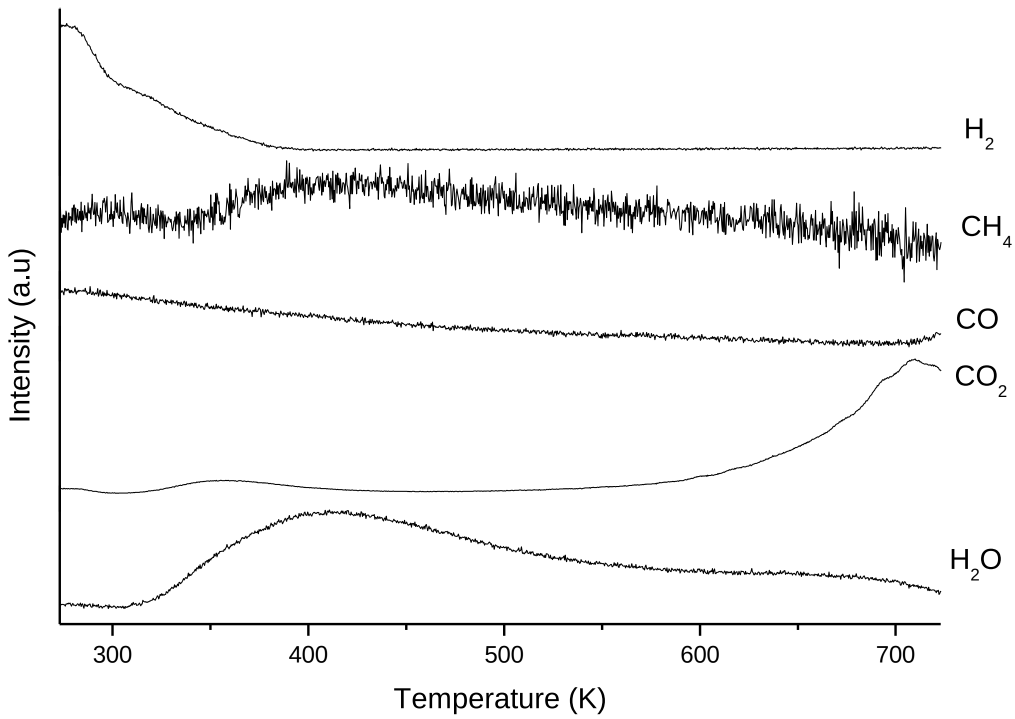

Figure 2. TPD of pre-adsorbed CO_2 at 298 K on 5%Ru/N-CNF.

To shed more light into the CO_2 reduction mechanism we performed temperature programmed surface reaction (TPSR) experiments (Figure 3). The formation of H_2O at low temperatures (peak around 370 K in Figures 3B and D) indicates that CO_2 flushed previously to TPSR dissociated as O_{ad} and a CO_{ad} species on Ru nanoparticle surface in agreement with TPD. In TPSR, O_{ad} species generates H_2O readily by reaction with H_{ad} species coming from the dissociation of H_2 present in gas phase.

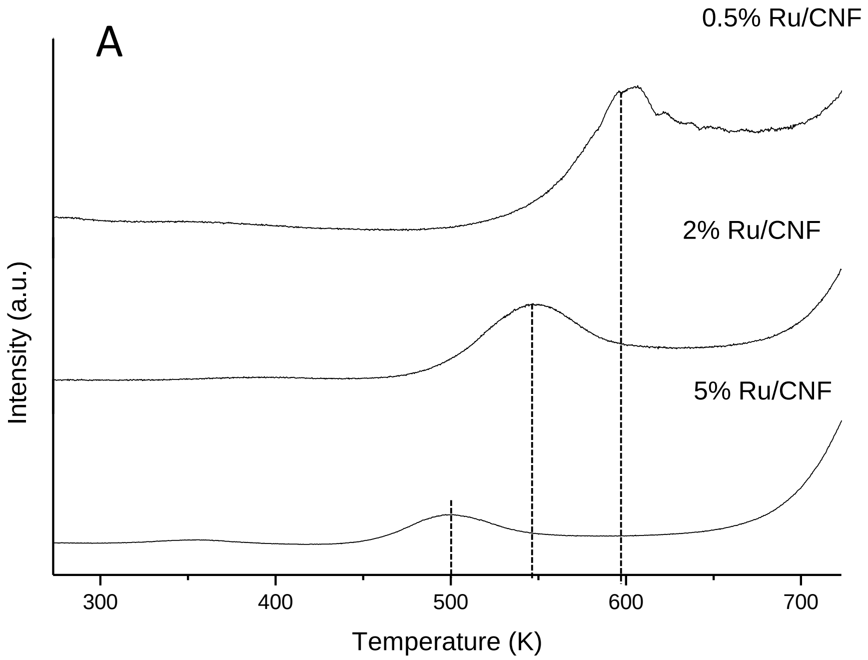
A
0.5% Ru/CNF
2% Ru/CNF
5% Ru/CNF
Intensity (a.u.)
300
400
500
600
700
Temperature (K)

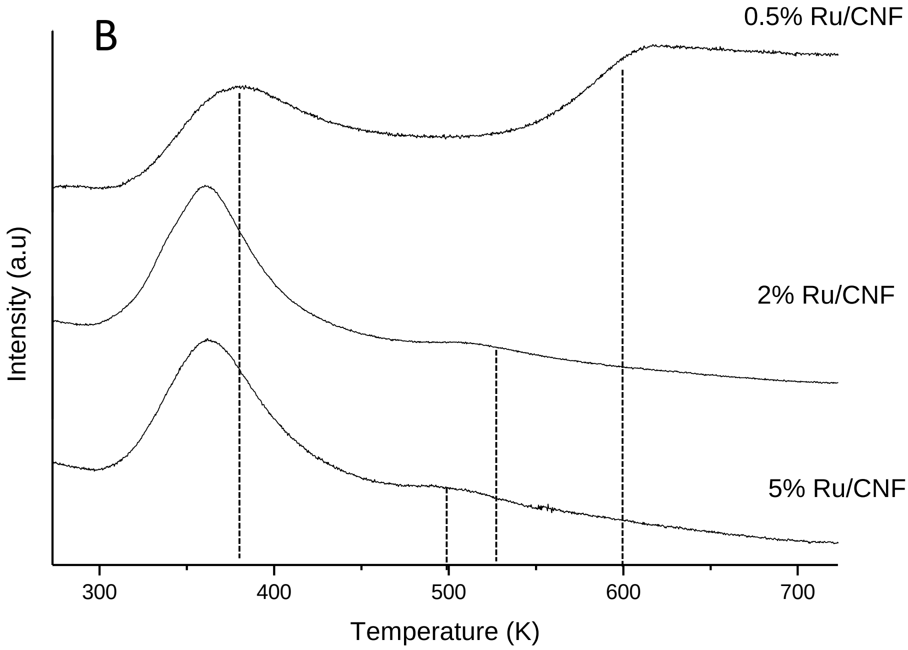
B
0.5% Ru/CNF
2% Ru/CNF
5% Ru/CNF
Intensity (a.u)
300
400
500
600
700
Temperature (K)

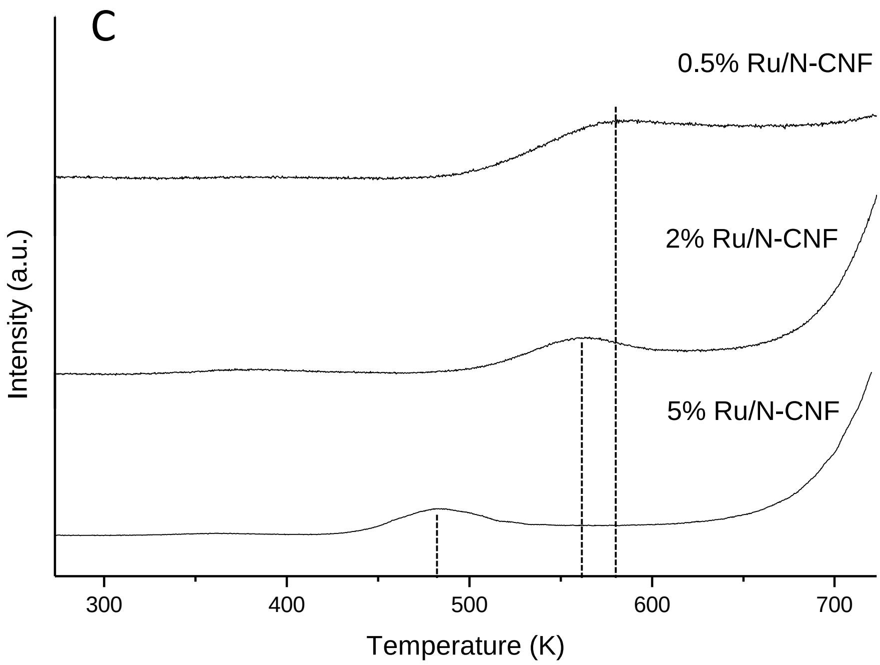

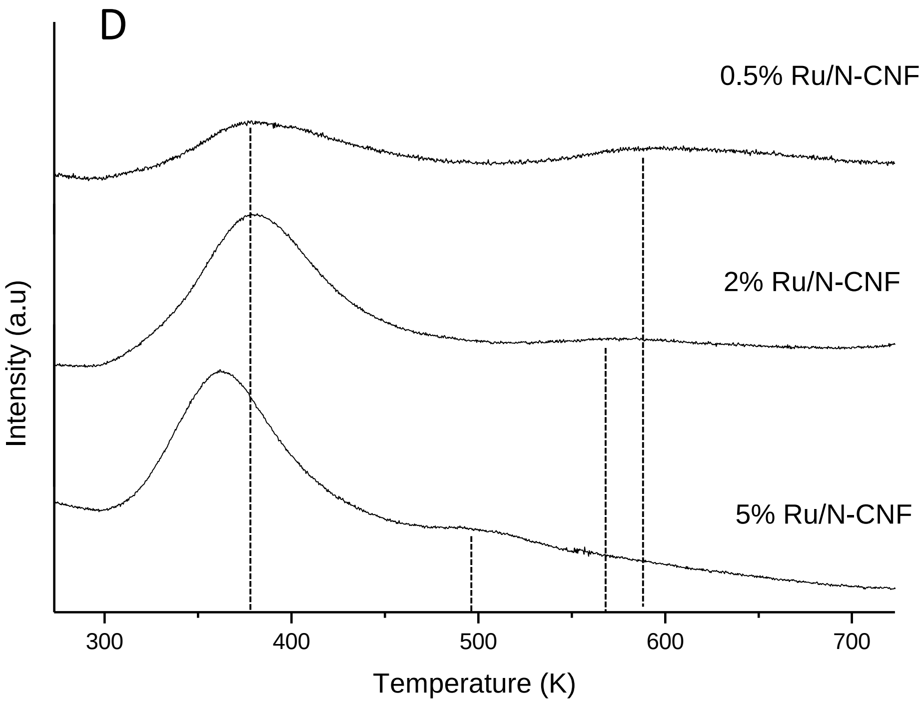

Figure 3. Signals of CH_4 (A, C) and H_2O (B, D) in temperature programmed surface reaction (TPSR) experiments using Ru on CNF (A, B) and Ru on N-CNF (C, D) containing different metal loadings.

In Figures 3 A and C, the peak corresponding to CH_4 formation is observed. The calibration of the CH_4 signal and the integration of the peak after subtracting baseline enabled the quantification of desorbed CH_4, which is compiled in Table 2. The moles of desorbed CH_4 give an indication of the CO_2 that has been dissociated and retained on the catalyst surface during CO_2 saturation at room temperature previous to TPSR. For catalysts evolving CH_4 at lower temperatures, *i.e.* those with higher Ru loadings, the quantified CH_4 can be unambiguously ascribed to the hydrogenation of CO_{ad} species, which were adsorbed previously. For catalysts containing the lowest loading (0.5 wt%), since the CH_4 peak occurs at high temperatures, it cannot be completely ruled out that part of quantified CH_4 stems from gasification of the support. Comparing the CH_4 produced in TPSR with the moles of Ru present on the catalyst (Table 2), it is apparent that the moles of CO_2 retained on the catalyst surface are almost one order of magnitude higher than the moles of Ru, suggesting that the support participates also on the storage of CO_{ad} coming from CO_2 dissociation. TPSR of the pristine supports after CO_2 pre-adsorption did not show desorption of any gas at temperatures below 673 K (Figure S1 of supplementary information), pointing out that the support needs the participation of ruthenium nanoparticles to dissociate CO_2 to species that are subsequently transferred to the support.

The peak of CH_4 formation in TPSR (Table 2 and Figures 3 A and C) occurs at decreasing temperatures as the Ru loading increases which is in agreement with the rising selectivity to CH_4. Moreover, the CH_4 peak is concomitant with a H_2O desorption peak indicating that the formation of at least part of CH_4 occurs *via* an oxygenated intermediate such as CO_{ad}.

Table 2. Quantification of TPSR and catalytic parameters

	Temperature of CH_4 peak K	Molar Ru loading mmol/g	CH_4 per catalyst weight in TPSR mmol/g	Molar CH_4/Ru ratio
0.5%Ru/CNF	606	0.049	3.75	76
2%Ru/CNF	557	0.20	2.37	12
5%Ru/CNF	500	0.50	4.08	8.2
0.5%Ru/N-CNF	575	0.05	1.93	39
2%Ru/N-CNF	559	0.19	1.16	5.8
5%Ru/N-CNF	481	0.49	3.14	6.3

Figure 4 shows the transient behaviour after the sudden removal of CO_2 from gas feed at three reaction temperatures for some selected catalysts. Similar experiments for the rest of catalysts are provided in Figures S2 and S3 of supporting material. It is a general behaviour of the catalysts that both CO_2 and CO signals decay as soon as CO_2 is removed from the gas feed. This suggests that the produced CO is released to gas phase directly by decomposition of CO_2 on the metal catalyst surface. On the other hand, CH_4 desorption shows a tail indicating that it is formed following a multistep process in which adsorbed intermediates are further hydrogenated until releasing CH_4. It is also noteworthy, that the CH_4 concentration in gas phase increases just when CO and CO_2 concentrations decay. CH_4 concentration reaches a maximum and then it declines because adsorbed CH_4-generating intermediates are depleted from catalyst surface. The CH_4 peak is less intense for higher reaction temperatures. For the same reaction temperatures, the maximum is more pronounced for 5%Ru/CNF (Figure 4 B) than for 5%Ru/N-CNF (Figure 4 A) and for a lower loading (2wt% Ru, Figure 4 C) more intense than for the higher loading (5 wt% Ru, Figure 4 B). The appearance of CH_4

peak seems to indicate that the rate determining step for CH_4 formation is the activation of H_2 and supply of 4 H_{ad} species to reduce the CO_{ad} intermediate. When CO_2 is removed from feed gas more Ru adsorption sites become available for the dissociative adsorption of H_2. This favours the supply of H_{ad} chemisorbed species to the CO_{ad} intermediate, enhancing CH_4 formation. This is consistent with the fact that the intensity of CH_4 peak exhibited an inverse relationship with the conversion at steady state, *i.e.* the peak is less intense for 5%Ru/N-CNF than for 5%Ru/CNF, for the higher loadings and for higher reaction temperatures. This later is consistent with the fact that the coverage of the metal by adsorbed species is lower at higher reaction temperatures, leaving more sites for H_2 chemisorption.

The H_2O signal (dashed line) in Figure 4 continues at the same concentration long time after removal of CO_2 from gas feed. Afterwards, the H_2O concentration decays to zero as observed in Figure 4 C and supplementary Figures S3 A and B. The holding up of H_2O formation after CO_2 removal should be due to the reaction of accumulated O_{ad} species with continuously fed H_{ad} species. The duration of H_2O formation thus has a direct relationship with the amount of reactive O_{ad} species on catalyst/support surface generated during previous CO_2 reduction reaction. The duration of H_2O formation increases as reaction temperature and Ru loading increase. These two factors favour higher CO_2 conversions and hence the building up of higher amount of O_{ad} species. The duration is also longer for CNF-supported catalyst than for N-CNF supported one (Figure S2 and S3 of supplementary information) which may suggest that CNF can lodge more adsorbed O_{ad} species than N-CNF. A reaction pathway is suggested in the discussion consistent with the results gathered during the transient experiments.

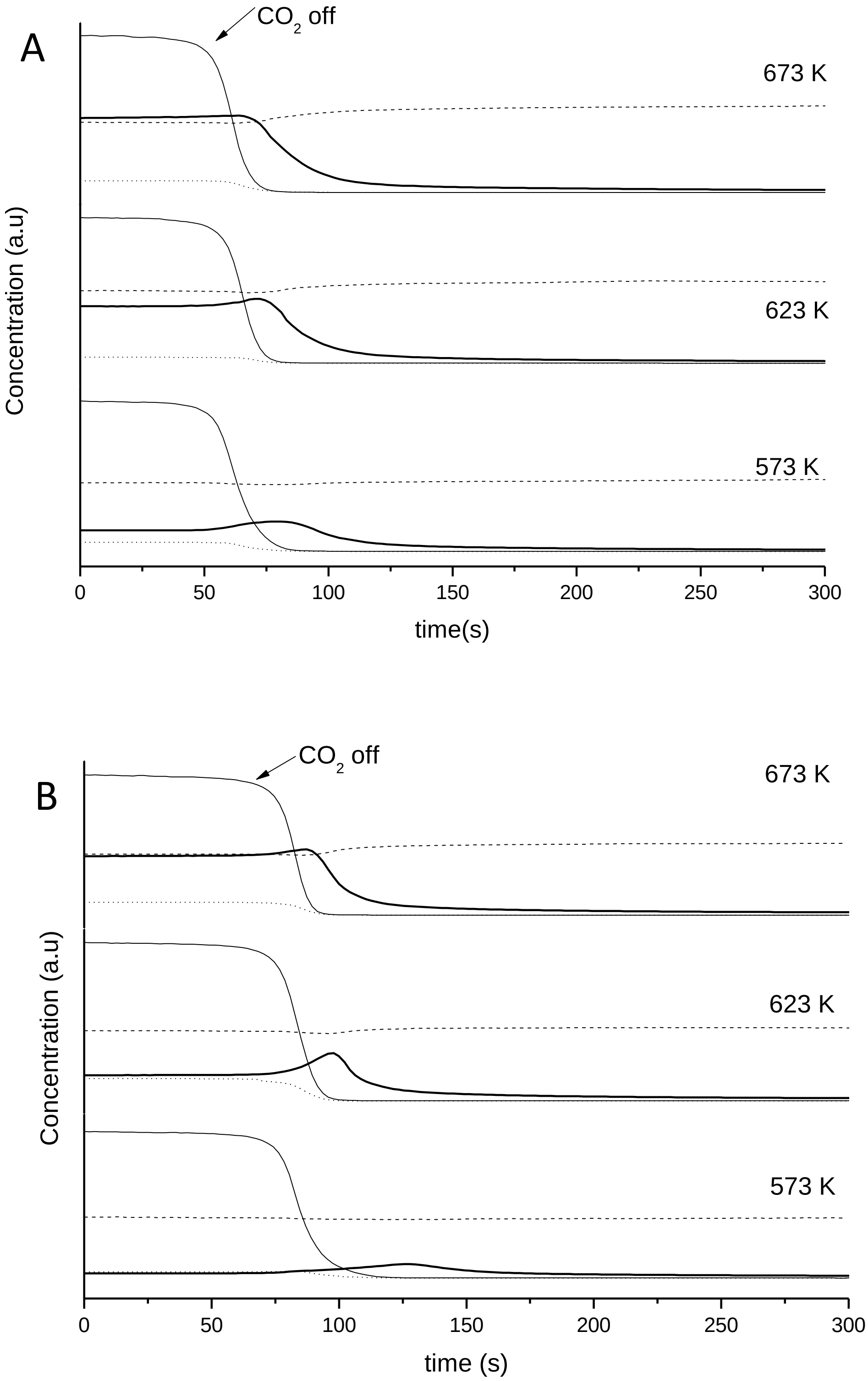
A
CO$_2$ off
673 K
623 K
573 K
Concentration (a.u)
0
50
100
150
200
250
300
time(s)
B
CO$_2$ off
673 K
623 K
573 K
Concentration (a.u)
0
50
100
150
200
250
300
time (s)

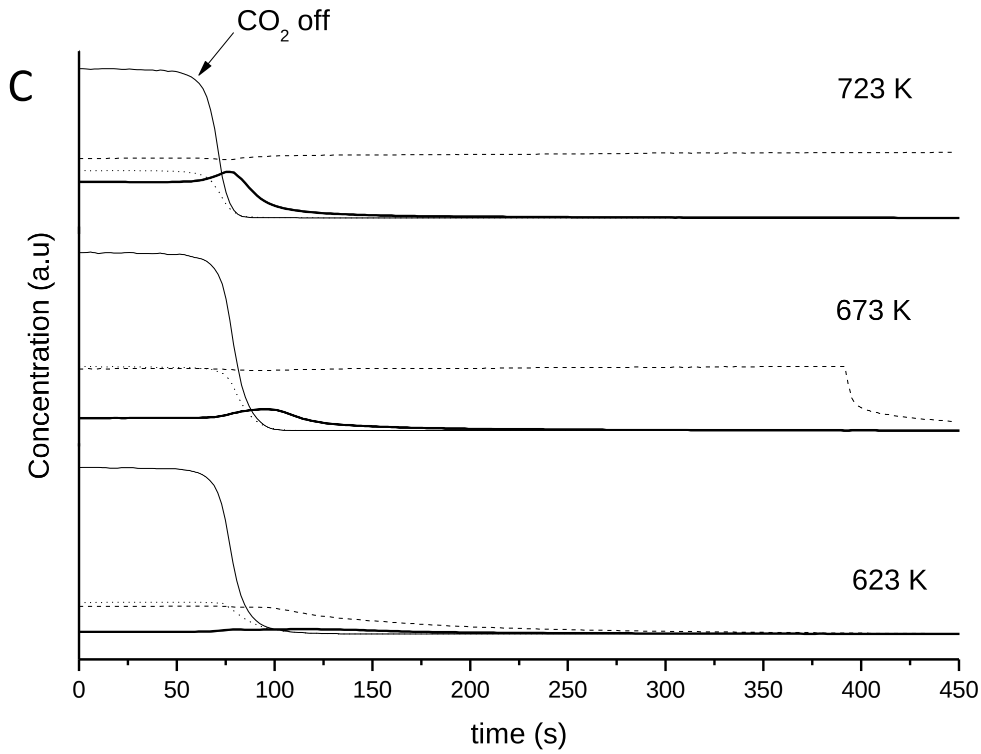

Figure 4. Experiments of transient response to CO_2 removal from the reaction mixture at three reaction temperatures for three selected catalysts: (A) 5%Ru/N-CNF catalyst, (B) 5%Ru/CNF catalyst, (C) 2%Ru/CNF catalyst. CO_2 concentration, thin solid line; CH_4 concentration, thick solid line; CO concentration, dotted line; H_2O concentration, dashed line. Feed gas composition: 5% CO_2, 15% H_2, Ar to balance.

To assess the stability, the catalyst with the highest activity, *i.e.* 5%Ru/N-CNF, was tested at the temperature of maximum CH_4 productivity, *i.e.* 623 K, during 20 hours reaction (Figure 5). The conversion even increased slightly with time on stream and the selectivity to CH_4 remained at constant values (>95 %). Additionally, long-term test was performed using a catalyst with the lowest Ru content, namely 0.5%Ru/N-CNF. This catalyst exhibited also an increase of conversion and the initial high selectivity to CO even increased further. Therefore, the catalysts are highly stable and the difference between their selectivities was even more accentuated after long-term testing.

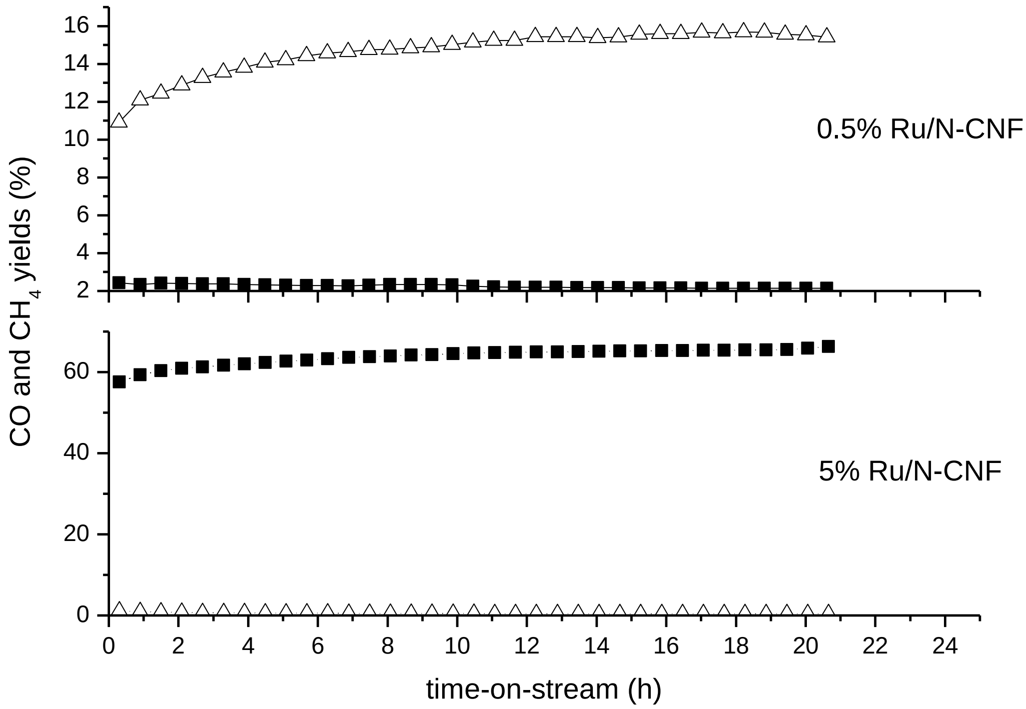

Figure 5. Long-term reaction stability tests with two catalysts containing different Ru loadings (0.5 and 5wt% Ru on N-CNF) and different selectivities at 623 K reaction temperature. **(■)** CH_4 yield (%), **(△)** CO yield (%).

3.2. TEM characterisation

We characterised the Ru particle size by STEM for the several prepared catalysts after reduction step at 723 K (Figure 6). For all the catalysts, more than 90% of the observed Ru particles had diameters smaller than 1.5 nm and no particles larger than 3.5 nm were found. Metal particles of sizes ranging from 2 to 3.5 nm were absent in catalysts containing 0.5 wt% Ru and were only between 4-9 % of total number of particles in catalysts containing 2 and 5 wt% Ru loadings. These two later catalysts showed very different selectivities to CH_4, despite their very similar particle size distribution. What is different between these two catalysts is the spatial distribution of the nanoparticles as observed in STEM images. For 2 wt% Ru loading, the nanoparticles are sparsely distributed while the Ru nanoparticles are closer to each other for 5 wt% Ru loading, leaving less support space between them.

Catalysts after stability test during 20 hours shown in Figure 5 were also characterized by STEM (Figure S4 supplementary information). The particle size distribution did not show significant change after long-term operation at 623 K, which is in line with the stable catalytic performance.

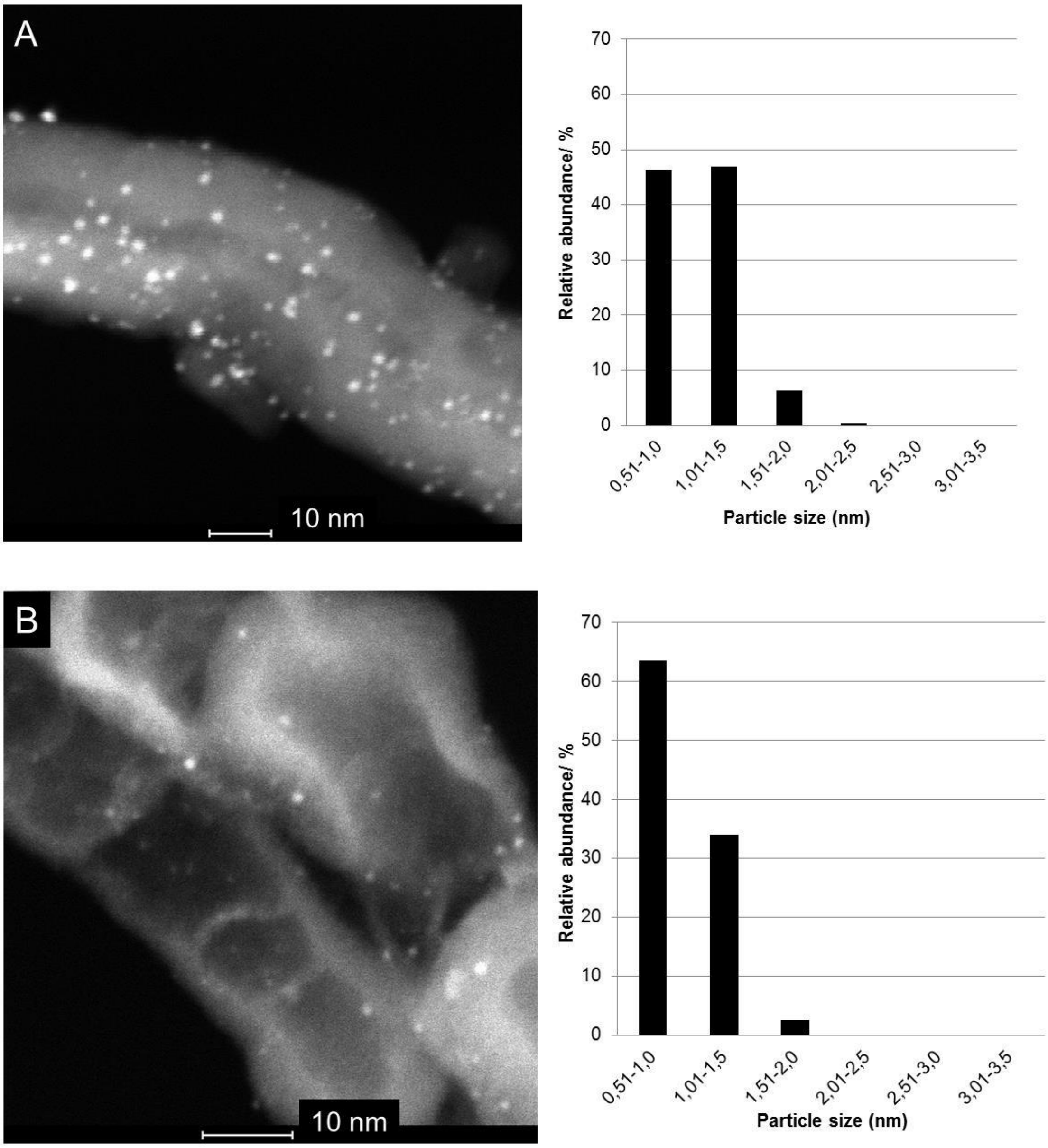

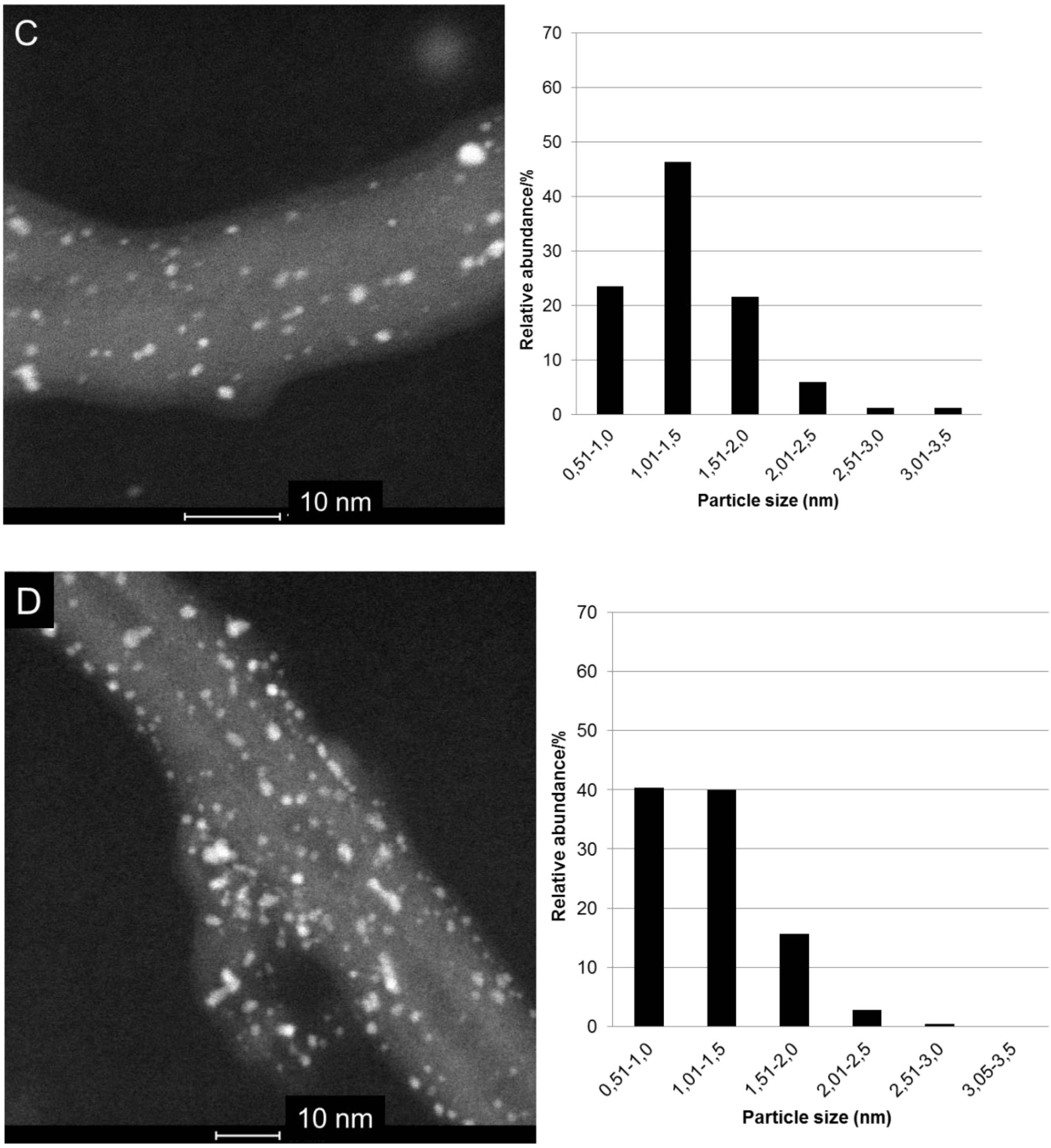
C
10 nm
Relative abundance/%
0
10
20
30
40
50
60
70
0,51-1,0
1,01-1,5
1,51-2,0
2,01-2,5
2,51-3,0
3,01-3,5
Particle size (nm)
D
10 nm
Relative abundance/%
0
10
20
30
40
50
60
70
0,51-1,0
1,01-1,5
1,51-2,0
2,01-2,5
2,51-3,0
3,05-3,5
Particle size (nm)

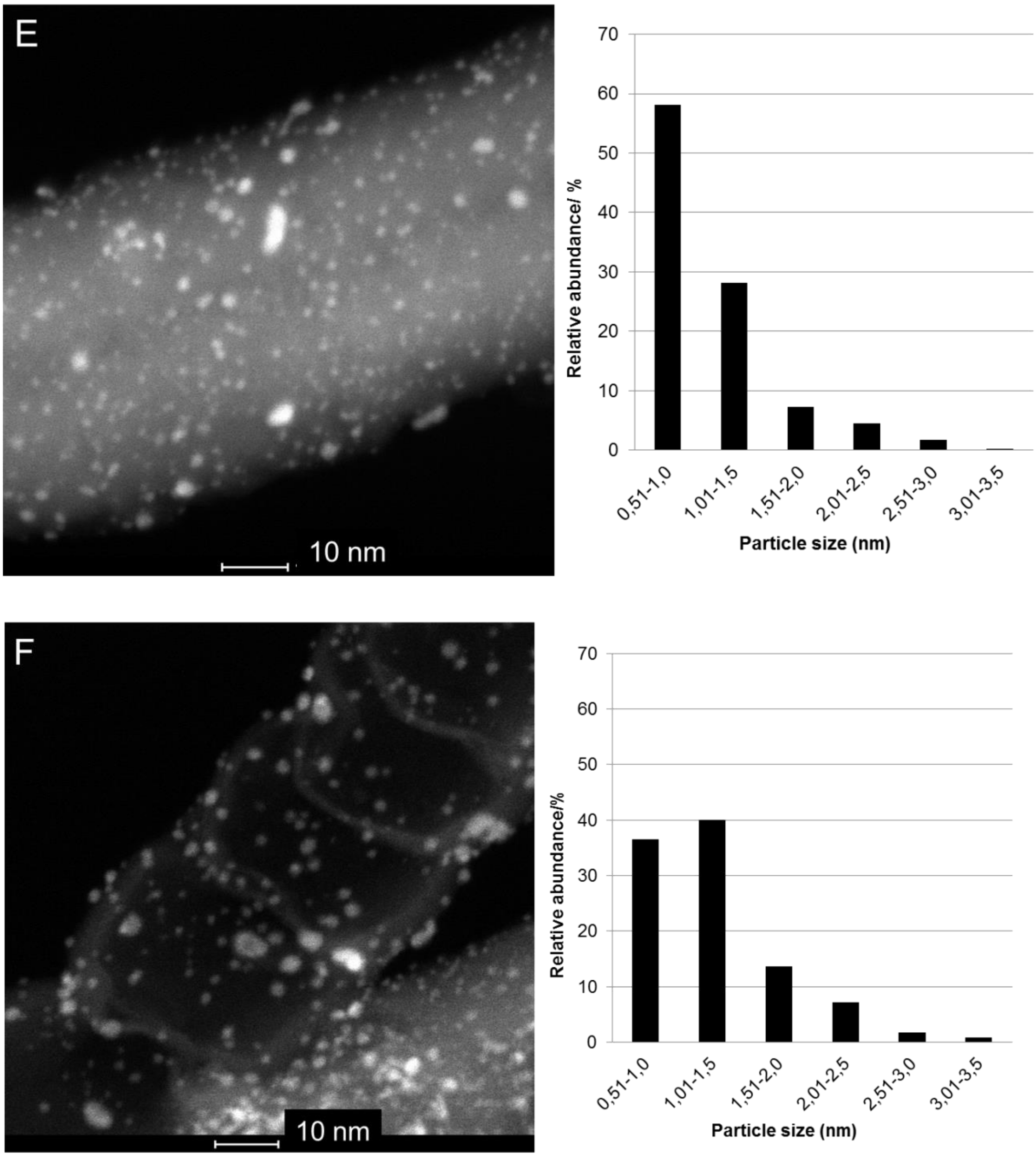

Figure 6. STEM images and particle size distribution of the different catalyst after reduction step at 723 K. (A) 0.5%Ru/CNF, (B) 0.5%Ru/N-CNF, (C) 2%Ru/CNF, (D) 2%Ru/N-CNF, (E) 5%Ru/CNF, (F) 5%Ru/N-CNF.

4. Discussion

The mechanism of CO_2 reduction to CH_4 on oxide-supported metal catalysts has been debated largely in the literature. Some authors propose that CO_{ad} is a key intermediate in the CO_2 methanation reaction and it is subsequently hydrogenated *via* the mechanism suggested for CO methanation. CO_{ad} can be formed *via* the reverse water gas shift through formate intermediate[17] or via dissociative CO_2 adsorption in a redox center.[41-43] Subsequently, the formation of CH_4 from CO_{ad} was proposed to proceed either by the initial C-O bond breaking[44-47] or with association of H_2 with CO_{ad} to form an intermediate and subsequent bond breaking.[48, 49]

On the basis of the results of transient experiments conducted here, the following reaction mechanism could be proposed. CO_2 is dissociated on reduced Ru nanoparticles even at room temperature and O_{ad} species and CO_{ad} species spilt over to the CNF support close to the interphase of metal nanoparticles. The dissociative chemisorption energies calculated in reference [50] for CO, CO_2 and H_2 on ruthenium are -1.62, -1.09 and -0.77 eV, respectively, with respect to molecules in vacuum. Therefore, CO is chemisorbed less strongly than CO_2 and H_2 on Ru nanoparticles and it can be displaced by the reactants towards the metal-support interphase, favouring the proposed spill over mechanism. The CO_{ad} species might be stored on the support due to some interaction with the edges of graphitic basal planes of CNF. The accumulation of O_{ad} species on support is evidenced by the formation of water at around 370 K in TPSR (Figure 3) and by the sustained formation of H_2O in transient response experiments after CO_2 removal from gas feed (Figure 4). The quantified moles of CH_4 produced in TPSR, which is one order of magnitude larger than moles of Ru, indicates that CO_{ad} intermediate species accumulated on the carbon support as well. The presence of Ru nanoparticles is necessary to dissociate CO_2 since no species were desorbed in TPSR using pristine supports (Figure S1 supplementary material). Some of the CH_4-generating intermediates are partially oxidised as inferred from the synchronous evolution of CH_4 and H_2O in TPSR. The nature of this CH_4-generating intermediate species is not clarified yet. Some authors have proposed the formation of reversible bicarbonates by reaction of CO_2 with the OH- groups of Al_2O_3 support.[31, 39] Similarly, bicarbonate species may be formed on OH- groups present on the edges of CNF basal planes. Contrarily, the mechanism of bicarbonate formation would hardly occur in the case of CNT support because exposed basal planes of CNT have fewer defects for CO_{ad} chemisorption. This would explain the negligible activity when CNTs are used as Pd catalyst support in the literature.[40]

The catalytic results showed that the selectivity pattern depends strongly on the metal loading. The selectivity is steered either towards CO for low Ru loadings or towards CH_4 for larger Ru loadings. Several authors found similar selectivity patterns as a function of the metal loading for different catalysts such as Ru on alumina,[30] Pd on alumina[40] or Ni on MCM-41.[10] Some of these authors attributed it to the different metal particle size, nano–sized metal clusters (2-5 nm) in 10% Pd on Al_2O_3 and atomically dispersed for 0.5 % Pd on Al_2O_3.[30, 40] In the other case,[10] sub-nanometer Ni cluster were reported irrespective of the metal loading and the size did not change after reaction. On the contrary, other authors observed an increase of CH_4 selectivity for smaller particles using Pd nanoparticles embedded in porous silica and ascribed this behaviour to the increased amount of corner and edge atoms.[51] Using nanoparticle model Co catalyst on silica, it was not observed any effect of particle size on selectivity to CH_4.[52] Therefore, it seems that there is not a particle size effect generalizable to all catalytic systems. In our case, we cannot attribute the different selectivity pattern to different Ru particle sizes because the differences in particle size distribution measured by STEM are inappreciable, especially between 2 wt% and 5 wt% Ru loaded catalysts. The main difference between those catalysts observed by STEM is that the Ru nanoparticles are closer for the highest Ru loading. Since the apparent particle size is very similar for all samples, those with higher Ru loading have also longer perimeter of interphase with the support. From the catalyst dispersion, the concentration of Ru on the perimeter was estimated (Table S1 supplementary material). Figure 7 shows that CH_4 yield exhibits a *quasi*-linear relationship with the concentration of Ru on the perimeter, especially for the catalyst supported on CNF. Similar importance of the metal catalyst perimeter has been previously reported for CO_2/CH_4 reforming to syngas using Pt/ZrO_2 catalyst.[26] It is claimed that CO_2 is activated *via* carbonate species on the support which must be in the proximity of the Pt particles to react with the methane activated on the metal.

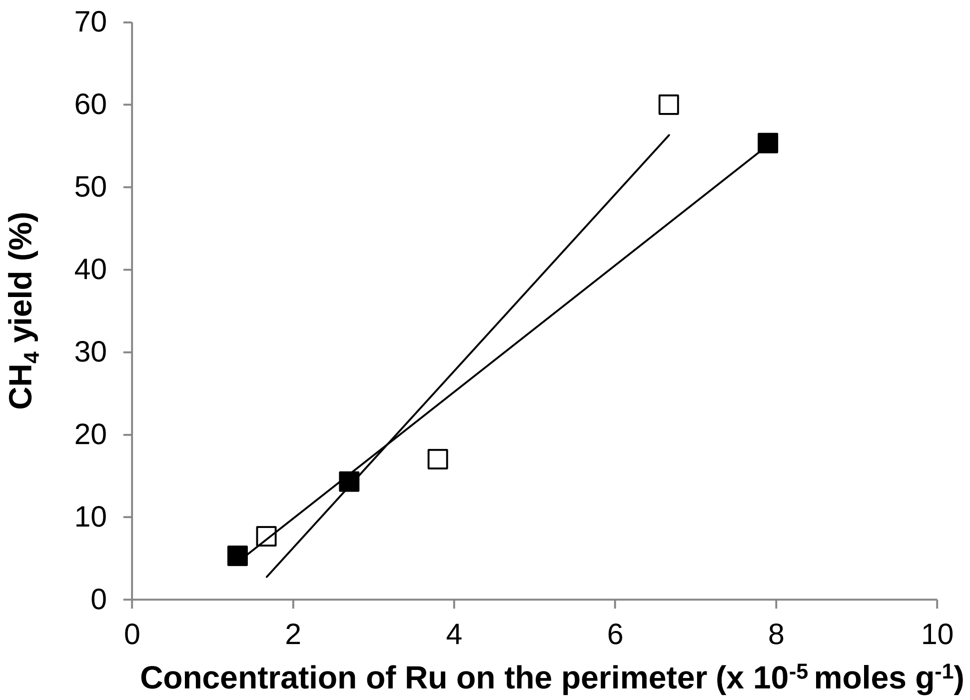

Figure 7. CH_4 yield at 673 K as a function of the concentration of Ru on the perimeter for the different Ru loadings supported either on CNF (■) or N-CNF (□).

According to the reaction mechanism proposed on the basis of transient experiments, the support would play a crucial role in the reaction. Therefore, a longer interphase perimeter between metal nanoparticles and support can be the reason of the different CH_4 selectivities. Since the supply of H_{ad} to the adsorbed CO_{ad} intermediate was found to be the rate determining step in transient response experiments (Figure 4), the closer proximity of Ru nanoparticles and larger interphase perimeter may also favour the supply of H_{ad} to the CO_{ad} intermediate and hence boosting the formation of CH_4. In fact, the CH_4 peak upon CO_2 removal in transient experiments almost vanished for catalyst exhibiting the highest activity at steady state, indicating that H_2 activation and H_{ad} supply is not that rate limiting in those cases. The overall reaction is governed by a subtle balance of adsorbed molecules, dissociated species and the reaction between them. Therefore, it is not straightforward to gather in one picture the whole process. For clarity, the simplified scheme of Figure 8 illustrates how different Ru loadings can affect the selectivity pattern. For the lower loadings (A), the metal particles are more separated and the supply of four H_{ad} to the activated CO_{ad} intermediate on the support is hindered. In contrast, for the highest loading the separation between nanoparticles is shorter and the supply of four H_{ad} atoms is enhanced.

The 5 wt% Ru catalyst supported on N-CNF outperforms its counterpart supported on CNF. Due to the several factors involved in this reaction, further research would be needed to unravel the exact reason of the enhanced performance of N-CNF supported catalyst. Transient response experiments (Figure 4 A and B) seem to indicate that the supply of H_{ad} active species is favoured for N-CNF supported catalyst. Additionally, the CH_4 desorption peak in TPSR of 5%Ru/N-CNF occurs at about 20 K lower temperature than that of 5%Ru/CNF which can be a result of the enhanced supply of H_{ad} or also to the formation of more reactive CO_{ad} intermediates upon CO_2 dissociation.

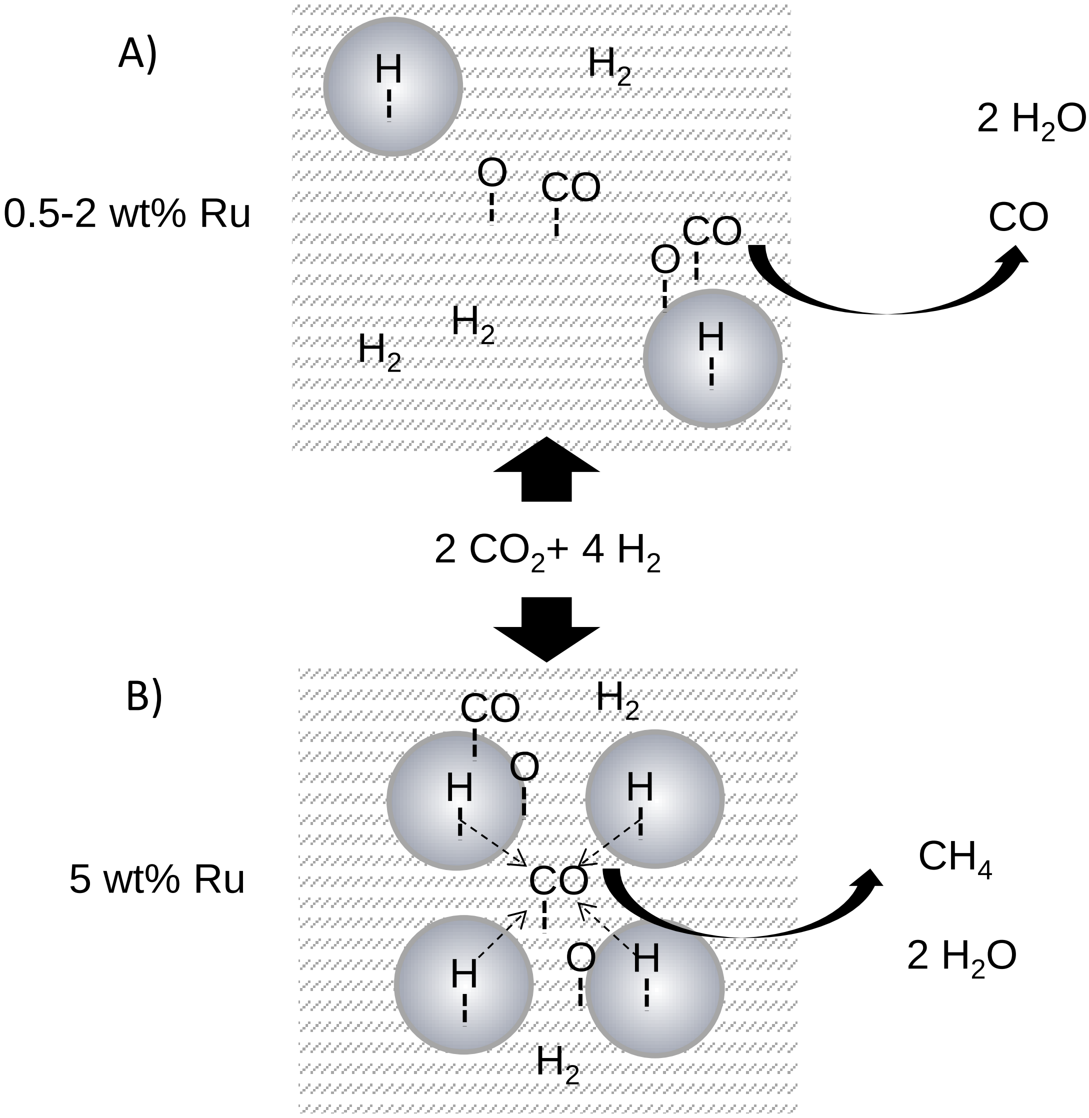

Figure 8. Scheme of different selectivity pattern depending on the different spatial separation of the Ru nanoparticles for the several Ru loadings. (A) hindered supply of H_{ad} for 0.5 and 2 wt% loaded catalyst. (B) Enhanced supply of H_{ad} to 5 wt% loaded catalyst.

The 5 wt% Ru on N-CNF catalyst showed activity comparable to catalyst supported on metal oxide supports reaching thermodynamic equilibrium conversion at 623 K and complete selectivity to CH_4 at a high space velocity (19000 h^{-1}). The catalyst is stable during long term operation, and the Ru particle size distribution remains constant after long term testing due to the strong attachment of Ru nanoparticles to the carbon support.

It has been recently reported that Ru nanoparticles on CNT are thermally stable keeping a high dispersion due to their anchoring *via* acetate ligands which are reconstructed after thermal treatment in the presence of oxygen.[53] Not all the metals supported on carbon nanotubes showed stability in CO_2 methanation. For instance, Ni supported on CNT catalyst tested in CO_2 methanation at 623 K during 6 hours showed a decrease of yield from 75% to 62% which was attributed to Ni sintering.[37]

Not only the catalyst here prepared outperforms other catalysts supported on carbon materials but it exhibits either superior CH_4 productivity than some of the best metal oxide supported catalysts tested in the literature under similar conditions (Table 3).

Table 3. Comparison of CH_4 productivity of this catalyst with some of the best catalysts in the literature tested under similar conditions.

entry	reference	catalyst	Loading wt%	Reaction temperature (K)	CH_4 productivity (mol $h^{-1}g_{metal}^{-1}$)
1	herein	Ru on N/CNF	5	643	1.9
2	[19]	Pd-Mg on SiO_2	6.2	723	0.5
3	[30]	Ru on Al_2O_3	5	643	1.7
4	[54]	Ni-Fe on Al_2O_3	23	523	0.8
5	[23]	Rh on Al_2O_3	1	423	0.4
6	[18]	Ru on CeO_2	5	723	0.05

7	[55]	Ni on USY	14	673	0.05

5. Conclusions

Ru supported on CNF or N-CNF showed remarkable activity and stability in the CO_2 reduction to CH_4, contrasting with the poor activity and selectivity reported for carbon nanotube supported catalysts. Moreover, the catalyst 5%Ru/N-CNF showed CH_4 productivity comparable to the best catalysts supported on metal oxides in the literature. Thus, the catalyst can be efficiently used in a CO_2 recycling process situated close to a place where renewable or by-product H_2 can be utilized.

To get insights about the reasons of this outstanding performance, catalytic transient response experiments were carried out. Transient experiments underscore the active participation of CNF and N-CNF support on the reaction as storage for reaction intermediate species. Thus the reaction occurs likely close to the interphase between Ru metal nanoparticles and support. The former assists the dissociation of H_2 to H_{ad} and of CO_2 to O_{ad} and a reduced intermediate CO_{ad} species. The dissociated species spilt over to the carbon support that functions as storage for O_{ad} and CO_{ad} species. Transient experiments revealed that CH_4 formation rate is controlled by the supply of 4 H_{ad} to the CO_{ad} intermediate. The selectivity depends strongly on the metal loading. For 0.5 and 2 wt% Ru loadings, the reduction is steered mainly to CO formation while for 5 wt% Ru loading the selectivity to CH_4 is 97 %. Since the Ru particle sizes did not differ significantly for catalysts containing different loadings, the different selectivity pattern cannot be ascribed to structure sensitivity. The higher selectivity to CH_4 is most likely explained by the enhanced supply of 4 H_{ad} to the activated CO_{ad} intermediate, which is favoured by the proximity between nanoparticles or to the longer interphase perimeter between metal nanoparticles and support.

Aknowledgements.

The financial support of European Commission (FREECATS project, FP7 Grant agreement nº 280658) from Spanish Ministry MINECO and the European Regional Development Fund (project ENE2013-48816-C5-5-R), and Regional Government of Aragon (DGA-ESF-T66 Grupo Consolidado) are gratefully acknowledged.

Supporting information statement

Temperature Programmed Surface Reaction (TPSR) experiments of the supports CNF and N-CNF. Experiments of transient response to CO_2 removal from gas feed for all catalysts. Representative STEM images and particle size distribution of catalysts 0.5 after testing for 20 hours at 623 K.

Reference List

[1] G. Centi, S. Perathoner. *Greenhouse Gas. : Sci. Tech.* **2011**, *1*(1), 21-35.

[2] *Energy Alliance for Hydrogen from Wind (http://www. performing-energy. de)* **2014**.

[3] G. A. Olah. *Angew. Chem. Int. Ed.* **2005**, *44*(18), 2636-2639.

[4] K. Hashimoto, M. Yamasaki, K. Fujimura, T. Matsui, K. Izumiya, M. Komori, A. A. El-Moneim, E. Akiyama, H. Habazaki, N. Kumagai, A. Kawashima, K. Asami. *Mater. Sci. Eng. : A* **1999**, *267*(2), 200-206.

[5] P. Sabatier. *Compt. Rend. Heb. Acad. Sci.* **1902**, *134*, 689-691.

[6] G. Centi, E. A. Quadrelli, S. Perathoner. *Ener. Environ. Sci.* **2013**, *6*(6), 1711-1731.

[7] E. V. Kondratenko, G. Mul, J. Baltrusaitis, G. O. Larrazabal, J. Perez-Ramirez. *Ener. Environ. Sci.* **2013**, *6*(11), 3112-3135.

[8] F. J. Fernandez-Alvarez, A. M. Aitani, L. A. Oro. *Catal. Sci. Technol.* **2014**, *4*(3), 611-624.

[9] J. M. Thomas. *ChemSusChem* **2014**, *7*(7), 1801-1832.

[10] G. Du, S. Lim, Y. Yang, C. Wang, L. Pfefferle, G. L. Haller. *J. Catal.* **2007**, *249*(2), 370-379.

[11] F. Studt, I. Sharafutdinov, F. Abild-Pedersen, C. F. Elkjær, J. S. Hummelshøj, S. Dahl, I. Chorkendorff, J. K. Nørskov. *Nat. Chem.* **2014**, *6*(4), 320-324.

[12] S. Tada, T. Shimizu, H. Kameyama, T. Haneda, R. Kikuchi. *Int. J. Hyd. Ener.* **2012**, *37*(7), 5527-5531.

[13] M. Tsuji, T. Kodama, T. Yoshida, Y. Kitayama, Y. Tamaura. *J. Catal.* **1996**, *164*(2), 315-321.

[14] G. Melaet, W. T. Ralston, C. S. Li, S. Alayoglu, K. An, N. Musselwhite, B. Kalkan, G. A. Somorjai. *J. Am. Chem. Soc.* **2014**, *136*(6), 2260-2263.

[15] R. E. Owen, J. P. O'Byrne, D. Mattia, P. Plucinski, S. I. Pascu, M. D. Jones. *Chem. Commun.* **2013**, *49*(99), 11683-11685.

[16] N. M. Gupta, V. S. Kamble, K. A. Rao, R. M. Iyer. *J. Catal.* **1979**, *60*(1), 57-67.

[17] M. R. Prairie, A. Renken, J. G. Highfield, K. Ravindranathan Thampi, M. Grätzel. *J. Catal.* **1991**, *129*(1), 130-144.

[18] S. Sharma, Z. Hu, P. Zhang, E. W. McFarland, H. Metiu. *J. Catal.* **2011**, *278*(2), 297-309.

[19] J. N. Park, E. W. McFarland. *J. Catal.* **2009**, *266*(1), 92-97.

[20] A. V. Boix, M. ü. A. Ulla, J. O. Petunchi. *J. Catal.* **1996**, *162*(2), 239-249.

[21] A. Boffa, C. Lin, A. T. Bell, G. A. Somorjai. *J. Catal.* **1994**, *149*(1), 149-158.

[22] C. De Leitenburg, A. Trovarelli. *J. Catal.* **1995**, *156*(1), 171-174.

[23] M. Jacquemin, A. Beuls, P. Ruiz. *Catal. Tod.* **2010**, *157*(1–4), 462-466.

[24] S. Scirè, C. Crisafulli, R. Maggiore, S. Minicò, S. Galvagno. *Catal. Lett.* **1998**, *51*(1-2), 41-45.

[25] E. E. Santiso, A. M. George, C. H. Turner, M. K. Kostov, K. E. Gubbins, M. Buongiorno-Nardelli, M. Sliwinska-Bartkowiak. *Appl. Surf. Sci.* **2005**, *252*(3), 766-777.

[26] J. H. Bitter, K. Seshan, J. A. Lercher. *J. Catal.* **1997**, *171*(1), 279-286.

[27] D. Li, N. Ichikuni, S. Shimazu, T. Uematsu. *Appl. Catal. A: Gen.* **1999**, *180*(1–2), 227-235.

[28] R. Büchel, A. Baiker, S. E. Pratsinis. *Appl. Catal. A: Gen.* **2014**, *477*(0), 93-101.

[29] C. Janke, M. S. Duyar, M. Hoskins, R. Farrauto. *Appl. Catal. B: Environ.* **2014**, *152–153*(0), 184-191.

[30] J. H. Kwak, L. Kovarik, J. Szanyi. *ACS Catal.* **2013**, *3*(11), 2449-2455.

[31] J. Szanyi, J. H. Kwak. *Phys. Chem. Chem. Phys.* **2014**, *16*(29), 15126-15138.

[32] M. R. Prairie, J. G. Highfield, A. Renken. *Chem. Eng. Sci.* **1991**, *46*(1), 113-121.

[33] Y. Traa. *Chem. eng. tech.* **1999**, *22*(4), 291-293.

[34] J. A. Rodriguez, J. Evans, L. Feria, A. B. Vidal, P. Liu, K. Nakamura, F. Illas. *J. Catal.* **2013**, *307*(0), 162-169.

[35] C. de Leitenburg, A. Trovarelli, J. Kašparb. *J. Catal.* **1997**, *166*(1), 98-107.

[36] M. C. Román-Martínez, D. Cazorla-Amorós, A. Linares-Solano, C. S.-M. de Lecea. *Appl. Catal. A: Gen.* **1994**, *116*(1–2), 187-204.

[37] Y. Feng, W. Yang, S. Chen, W. Chu. *Integr. Ferroelec.* **2014**, *151*(1), 116-125.

[38] J. P. O'Byrne, R. E. Owen, D. R. Minett, S. I. Pascu, P. K. Plucinski, M. D. Jones, D. Mattia. *Catal. Sci. Tech.* **2013**, *3*(5), 1202-1207.

[39] C. J. Keturakis, F. Ni, M. Spicer, M. G. Beaver, H. S. Caram, I. E. Wachs. *ChemSusChem* **2014**, *7*, 3459-3466.

[40] J. H. Kwak, L. Kovarik, J. Szanyi. *ACS Catal.* **2013**, *3*(9), 2094-2100.

[41] K. H. Ernst, C. T. Campbell, G. Moretti. *J. Catal.* **1992**, *134*(1), 66-74.

[42] L. F. Liotta, G. A. Martin, G. Deganello. *J. Catal.* **1996**, *164*(2), 322-333.

[43] W. Wang, S. Wang, X. Ma, J. Gong. *Chem. Soc. Rev.* **2011**, *40*(7), 3703-3727.

[44] A. Bell. *Catal. rev. . Sci. eng.* **1981**, *23*(1-2), 203-232.

[45] D. W. Goodman, R. D. Kelley, T. E. Madey, J. Yates. *J. Catal.* **1980**, *63*(1), 226-234.

[46] N. M. Gupta, V. P. Londhe, V. S. Kamble. *J. Catal.* **1997**, *169*(2), 423-437.

[47] H. H. Nijs, P. A. Jacobs. *J. Catal.* **1980**, *66*(2), 401-411.

[48] M. P. Andersson, F. Abild-Pedersen, I. N. Remediakis, T. Bligaard, G. Jones, J. Engbæk, O. Lytken, S. Horch, J. H. Nielsen, J. Sehested, J. R. Rostrup-Nielsen, J. K. Nørskov, I. Chorkendorff. *J. Catal.* **2008**, *255*(1), 6-19.

[49] I. A. Fisher, A. T. Bell. *J. Catal.* **1996**, *162*(1), 54-65.

[50] T. Bligaard, J. K. Nørskov, S. Dahl, J. Matthiesen, C. H. Christensen, J. Sehested. *J. Catal.* **2004**, *224*(1), 206-217.

[51] J. Martins, N. Batail, S. Silva, S. Rafik-Clement, A. Karelovic, D. P. Debecker, A. Chaumonnot, D. Uzio. *Catal. Comm.* **2015**, *58*(0), 11-15.

[52] G. Melaet, A. Lindeman, G. Somorjai. *Top Catal* **2014**, *57*(6-9), 500-507.

[53] B. F. Machado, M. Oubenali, M. Rosa Axet, T. Trang NGuyen, M. Tunckol, M. Girleanu, O. Ersen, I. C. Gerber, P. Serp. *J. Catal.* **2014**, *309*(0), 185-198.

[54] J. Sehested, K. Larsen, A. Kustov, A. Frey, T. Johannessen, T. Bligaard, M. Andersson, J. Nørskov, C. Christensen. *Top Catal* **2007**, *45*(1-4), 9-13.

[55] I. Graça, L. V. González, M. C. Bacariza, A. Fernandes, C. Henriques, J. M. Lopes, M. F. Ribeiro. *Appl. Catal. B: Environ.* **2014**, *147*(0), 101-110.

TABLE OF CONTENTS

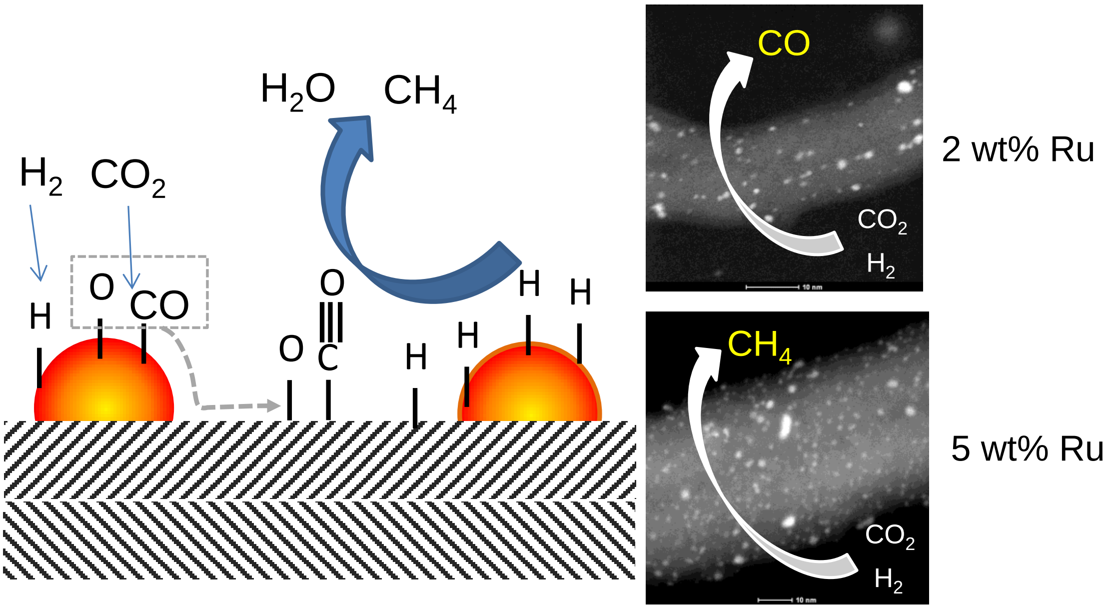

N-doped carbon nanofibers demonstrated to be an effective support of Ru nanoparticles for the reduction of CO_2 to CH_4. Higher loadings favoured the selectivity to CH_4. The catalyst support not only helps to stabilise Ru nanoparticles but also participates actively in reaction mechanism.